The FASEB Journal

FASEB
Federation of American Societies for Experimental Biology

RESEARCH ARTICLE

Short-Term Rapamycin Mitigates the Senescence of Ovaries and Somatic Stem Cells in Multiple Organs in Reproductively Aged Mice

Jiangtao Lu[1,2] | Jie Li[1,2] | Chang Liu[1,2] | Guofeng Feng[1,2] | Guoxing Yin[1,2] | Ziyue Hu[1,2] | Dai Heng[1,2] | Yongqin Yu[1,2] | Kairang Jin[1,2] | Yiwei Wu[1,2] | Zhuangzhuang Feng[1,2] | Junru Chen[1,2] | Yufei Wei[1,2] | Yating Wang[1,2] | Xuemin Hu[3] | Lin Liu[1,2] | Xue Du[3] | Zhengmao Zhu[1,2]

[1]State Key Laboratory of Medicinal Chemical Biology, Nankai University, Tianjin, China | [2]Department of Cell Biology and Genetics, Nankai University, Tianjin, China | [3]Department of Gynecology, Tianjin, Union Medical Center, The First Affiliated Hospital of Nankai University, Tianjin, China

Correspondence: Xue Du (lanlandetommao@163.com) | Zhengmao Zhu (zhuzhengmao@nankai.edu.cn)

Received: 4 November 2025 | **Revised:** 27 January 2026 | **Accepted:** 2 February 2026

Keywords: ovarian senescence | rapamycin | reproductive aged mice | somatic stem cells

ABSTRACT

Reproductive aging in females is marked by ovarian senescence and a concomitant decline in somatic organ function. Mechanistic target of rapamycin (mTOR) signaling is a central regulator of aging. Rapamycin has been shown to confer anti-aging benefits in young and middle-aged females; however, whether mTOR inhibition remains effective once reproductive aging is established remains unclear. Here we analyzed transcriptomics of oocytes and granulosa cells from reproductively aged (10-month-old) mice and identified upregulation of ribosome biogenesis and cytoplasmic translation, consistent with hyperactive mTOR signaling. We then evaluated the effects of short-term rapamycin treatment during the perimenopausal period. One month of rapamycin treatment effectively suppressed mTOR signaling and reduced cellular senescence, inflammation, fibrosis, and oxidative damage in the ovary, lung, small intestine, and skeletal muscle. Rapamycin also alleviated somatic stem exhaustion across multiple tissues by reducing DNA damage and senescence markers, restoring stem cell abundance, and improving differentiation capacity. Despite these improvements in the somatic microenvironment, rapamycin failed to restore fertility or serum estradiol levels in reproductively aged females. Importantly, the beneficial effects on mTOR activity, stem cell function, and tissue homeostasis were largely reversed following treatment withdrawal. Together, our findings demonstrate that short-term mTOR inhibition initiated after reproductive aging can transiently ameliorate systemic and ovarian aging phenotypes while highlighting a key limitation: reproductive function is not recoverable once advanced reproductive aging has occurred. And these results indicated the importance of intervention timing and suggest the therapeutic scope of rapamycin during female reproductive aging.

1 | Introduction

Aging is a complex process characterized by increased age-related diseases and decreased physiological functions [1, 2]. Perimenopausal women experience a decline in fertility, associated with ovarian functional decline due to aging [3, 4], and increased risks of age-related chronic diseases in somatic organs, such as endocrine dysfunction, digestive disorders,

Jiangtao Lu and Jie Li have contributed equally to this work.

Xue Du and Zhengmao Zhu have contributed equally to this work.

and cardiovascular diseases [5]. Aging also impairs stem cell function, disrupting tissue regeneration and homeostasis [6, 7]. Targeting conserved biological mechanisms may offer therapeutic strategies to regulate aging and its effects [8].

Dietary restriction (DR) extends the lifespan of mice, but it can also adversely affect other aspects of physiological health [9]. In rodents, chronic caloric restriction (CR) often suppresses ovarian follicular development and causes irregular estrous cycles, leading to subfertility or infertility [10]. These adverse effects indicate a critical limitation of CR in the context of female reproductive aging. Therefore, interventions that can extend healthspan without impairing reproductive function are of particular interest. Pharmacological inhibition of mTOR, a conserved nutrient-sensing pathway downstream of DR [11, 12], has emerged as a promising alternative strategy. Rapamycin recapitulates several beneficial effects of DR on longevity and tissue homeostasis without the need for severe CR, making it attractive for studying aging interventions in females [13, 14]. These preclinical findings are supported by human data: a systematic review by Andrea B. Maier et al. concluded that rapamycin and its analogs enhance immune, cardiovascular, and integumentary functions in healthy individuals or those with aging-related conditions, while no significant effects were observed on the endocrine, muscular, or neurological systems; the impacts on the respiratory, digestive, renal, and reproductive systems remain unevaluated [15]. Importantly, in women aged 30–50 years, functional decline in organs such as the liver, lung, skeletal muscle, and bone is closely associated with aging [16], and accumulating evidence indicates that age-related exhaustion of stem and progenitor cells in the lung [17, 18], small intestine [19], and skeletal muscle [20] results in part from repeated activation of mTORC1 signaling during tissue regeneration. Although short-term (2 weeks) rapamycin treatment has been shown to delay ovarian aging in young and middle-aged female mice [10], whether mTOR inhibition remains effective once reproductive aging is already established remains unknown. In female mice, reproductive aging typically occurs at 10–12 months of age, a stage characterized by progressive reproductive cycle irregularity that ultimately leads to complete cessation of cyclicity [21], but preceding overt systemic aging.

This life stage corresponds to the perimenopausal transition (45–55 years old) in women, which is increasingly recognized as a period of accelerated physiological decline and heightened vulnerability to age-associated diseases [1, 16]. Given that perimenopause represents a period of accelerated systemic aging in women, it is critical to examine whether mTOR inhibition remains effective when initiated after reproductive decline has already begun. This study investigated whether short-term rapamycin treatment during the perimenopausal period could alleviate aging in the ovary, lung, small intestine, and skeletal muscle. We found that in 10–12-month-old female mice, such treatment delayed ovarian senescence, reduced inflammation and age-related marker levels across multiple tissues, and enhanced somatic stem cell function in the lung, small intestine, and skeletal muscle. Although these anti-aging benefits persisted beyond the treatment period compared with untreated controls, the effects on mTOR signaling, stem cell activity, and tissue differentiation diminished after drug withdrawal.

2 | Materials and Methods

2.1 | Animals

Female C57BL/six mice, aged 2 months (young) and 10 months (Throughout this study, the term "reproductively aged" refers to 10–12-month-old female mice that exhibit reproductive decline but have not yet entered overt physiological aging.), were acquired from Beijing Vital River Laboratory Animal Technology Co. Ltd. All the mice were housed individually in ventilated cages (IVCs) under a 12-h light/dark cycle within the sterile Animal Facility at the College of Life Sciences. The study was approved by the Nankai University Animal Care and Use Committee, and all procedures adhered to established guidelines and relevant regulations.

Rapamycin treatment was conducted as previously described [22]. Briefly, rapamycin (LC Laboratories, R-5000) was prepared in DMSO at a concentration of 100 mg mL-1. The 10-month-old female mice received either DMSO or rapamycin in the drinking water at a final concentration of 40 mg/L1 (approximately 8.0 mg kg-1 day-1) [22, 23] for 30 days. After this treatment period, all the groups were switched to plain drinking water until they reached 12 months of age. To induce superovulation, all the groups received an injection of 5 IU pregnant mare serum gonadotrophin (PMSG), followed by 5 IU human chorionic gonadotrophin (hCG) 46–48 h later, for the collection and quality analysis of MII oocytes.

2.2 | Western Blot

After centrifugation at 10000 × g for 10 min at 4°C, the supernatant was transferred into new tubes. The protein concentration was determined via a bicinchoninic acid assay, and the samples were boiled in SDS sample buffer at 100°C for 10 min. Proteins from each cell extract were separated via 10% Acr-Bis SDS–PAGE and transferred to polyvinylidene difluoride (PVDF) membranes (Millipore). The membranes were blocked with 5% skim milk in TBST for 2 h at room temperature, followed by overnight incubation with primary antibodies at 4°C. β-actin served as a loading control. The immunoreactive bands were then incubated for 2 h at room temperature with HRP-conjugated secondary antibodies. The protein bands were visualized via a chemiluminescent HRP substrate (WBKLS0500, Millipore). The antibodies used for western blotting included p-S6 (4858S, Cell Signaling Technology), S6 (2217S, Cell Signaling Technology), α-SMA (ab5694, Abcam), IL-1β (sc-52 746, Santa Cruz Biotechnology), TNF-α (sc-52 746, Santa Cruz Biotechnology), Cxcl2 (HA723640, HUABIO), p16INK4A (sc-1661, Santa Cruz Biotechnology) and β-actin (AC026, ABclonal).

2.3 | SA-β-Gal Staining

senescence-associated β-galactosidase (SA-β-gal) staining was performed via a senescence-associated β-galactosidase staining kit (Beyotime, China, C0602) following the manufacturer's instructions and a previously described method [24]. Briefly, granulosa cells and ovarian sections were washed three times with PBS, fixed in 4% paraformaldehyde for 15 min at room

temperature, and then washed again three times with PBS. The samples were incubated overnight in the dark at 37°C with a mixture containing 5-bromo-4-chloro-3-indolyl-b-d-galactopyranoside (X-gal).

2.4 | H&E Staining

Hematoxylin and eosin (H&E) staining was performed as previously described [10]. Paraffin-embedded tissue sections were sliced to a thickness of 5 μm. The sections were dewaxed in xylene and then rehydrated through a series of alcohol concentrations (100%, 100%, 95%, 90%, 80%, 70%, and 50%), followed by brief rinsing in distilled water. The slices were incubated in hematoxylin solution until the desired staining level was reached (Beyotime, China) and rinsed in tap water to eliminate excess hematoxylin. The slices were then differentiated in 1% acid alcohol for 1–2 s, followed by a 1-min rinse in running water. Finally, the slices were covered with Cytoseal-60 (Solarbio, China) for preservation.

2.5 | Masson's Staining

Tissue sections embedded in paraffin were first deparaffinized in 100% xylene and then rehydrated through a series of alcohols (100%, 95%, 90%, 80%, and 70%). After a 5-min wash in distilled water, the sections were stained overnight with potassium bichromate and rinsed under running water for 5–10 min. They were then treated with Weigert's iron hematoxylin solution for 10 min, followed by rinsing in warm running water for 10 min. Next, the sections were stained with Ponceau-acid fuchsin for 5–10 min, washed in distilled water, and differentiated in phosphomolybdic-phosphotungstic acid for 10–15 min. Without rinsing, the sections were transferred directly to aniline blue solution for 5–10 min, briefly rinsed in distilled water and differentiated in 1% acetic acid for 2–5 min. The sections were washed three times in distilled water for 5 min each, dehydrated through an ethanol gradient (70%, 80%, 90%, 100%, and 100%), treated with 100% xylene, and finally mounted in a resinous medium.

2.6 | Estradiol (E2) Assays

Serum estradiol (E2) levels were detected by ELISA Kit (CK-E20419 Hangzhou Eastbiopharm Co. Ltd) [22]. Quality control serum, sterilized distilled water, and five series diluted standard samples for a standard curve were tested for each serum sample. The intra- and inter-assay coefficients of variability for E2 were below 8% and 12%.

2.7 | Isolation and Culture of Mouse Granulosa Cells

Mouse granulosa cells (mGCs) were isolated and cultured following previously established protocols [25, 26]. Briefly, PMSG was injected into the abdominal cavity of mice 46 h before isolating mGCs. The mice were humanely sacrificed, and the ovaries were dissected. Insulin syringes were used to puncture visible follicles on the surface of the ovaries under a stereomicroscope to release mGCs into culture medium, avoiding isolation of mGCs from small follicles. In addition, oocytes were filtered out using a 40-μm cell strainer (Falcon). Then, the isolated mGCs were washed three times and seeded in culture medium.

2.8 | Histopathological Analyses and Immunostaining

For ovarian frozen sections, the samples were washed in PBS for 10 min, fixed in ice-cold acetone at room temperature for 15 min, treated with 0.1% Triton X-100 for 1 h, and blocked with 3% BSA in PBS for 2 h at room temperature. The samples were incubated overnight with primary antibodies at 4°C, followed by three washes with PBS for 15 min each. The sections were incubated for 2 h with an appropriate fluorescence-conjugated secondary antibody (donkey anti-rabbit IgG Alexa Fluor 594 antibody, 1:200, A-21207, Thermo Scientific), washed three times in PBS, and counterstained with 5 $\mu g\,mL^{-1}$ Hoechst 33342 in Vectashield (H-1000-10, VectorLabs) mounting medium. Fluorescence imaging was performed via an Axio Imager Z2 fluorescence microscope (Carl Zeiss), and ImageJ was used for relative fluorescence quantification.

For histopathological analyses and immunostaining, 5-μm sections from the paraffin-embedded lung, small intestine, and skeletal muscle were prepared. The following antibodies were used: anti-p-mTOR antibody (2971 s, 1:100; Cell Signaling Technology), anti-p-S6 antibody (4858S, 1:100; Cell Signaling Technology), anti-CDKN2A/p16INK4A antibody (sc-1661, 1:200; Santa Cruz Biotechnology), anti-TNF-α antibody (sc-52 746, 1:200; Santa Cruz Biotechnology), anti-IL-1β antibody (sc-52 012, 1:50; Santa Cruz Biotechnology), anti-8-OHdG antibody (sc-66 036, 1:150; Santa Cruz Biotechnology), anti-α-SMA antibody (ab5694, 1:100; Abcam), anti-pro-surfactant protein C (ab211326, 1:300; Abcam), anti-LGR5 antibody (DF2816, 1:100; Affinity), anti-PAX7 antibody (sc-81 975, 1:50; Santa Cruz Biotechnology), anti-phospho-histone H2AX antibody (Ser139, 1:100; ABclonal), anti-PCNA antibody (sc-25 280, 1:100; Santa Cruz Biotechnology), and anti-HOPX antibody (sc-398 703). Images were acquired via Thunder and SP8 fluorescence microscopes (Leica). Histological quantifications were performed randomly on five different areas per case via the Fiji software package (http://fiji.sc) to measure the total number and percentage of DAB-positive areas.

2.9 | Quantitative PCR (qPCR) of RNAs

Total RNA from cumulus cells was extracted with a RNeasy RNA Micro Kit (74 034, QIAGEN) following the manufacturer's instructions. Purified total RNA was reverse transcribed to generate cDNA via M-MLV reverse transcriptase (Invitrogen) and random hexamer primers as instructed. For a single oocyte, mRNA was directly reverse transcribed to cDNA via

Smart-seq2, and the resulting product was used for qPCR. qPCR was performed with FastStart Universal SYBR Green Master Mix (4913914001, Roche) on an iCycler MyiQ2 detection system (Bio-Rad). Each sample was prepared in duplicate and normalized against *GAPDH*. The qPCR data were analyzed via the ΔΔCt method, and the specificity of the primers (Table S1) was verified through dissociation curves.

2.10 | Quantitative Analysis of Serum Cytokines and Chemokines

Cytokines and chemokines in mouse serum were measured via the ABplex Mouse Plex Custom Panel (ABclonal, RK04397) according to the manufacturer's instructions [27]. These include IL-1β, TNF-α, IL-12 (p40), IL-4, IL-5, IL-10, VCAM-1, IFN-γ, IL-12 (p70), IL-17A, IL-2, IL-1α, and IL-3. Data analysis was performed with Multiplex Analyst Software from ABclonal.

2.11 | TUNEL Assay

The paraffin-embedded sections were stained with TUNEL reagent according to the manufacturer's protocols, and images were captured with a fluorescence microscope (Leica, Wetzlar, Germany).

2.12 | AB-PAS Staining

Intestinal tissues were fixed in 4% paraformaldehyde in PBS, embedded in paraffin, sectioned, and stained with AB-PAS (Solarbio, China) according to the manufacturer's instructions. Images of the sections were captured to quantify the number of goblet cells per villus.

2.13 | Single-Cell RNA-Seq Data Analysis

The transcriptomic analysis was based on a re-analysis of our previously published dataset (GSE184637). Specifically, this dataset includes SMART-seq2 data from 18 MII oocytes collected from 2-month-old mice and 20 MII oocytes from 10-month-old mice. For cumulus cells, ovaries were obtained from three mice per age group (2 and 10 months). Mice were intraperitoneally injected with PMSG 46 h before GC isolation. After humane euthanasia, ovaries were dissected, and visible follicles on the ovarian surface were punctured under a stereomicroscope using insulin needles to release GCs into the culture medium, avoiding small follicles. Oocytes were removed by filtration through a 40-μm cell strainer. The isolated GCs were then washed with phosphate-buffered saline, dispersed into single-cell suspensions, and 50 cells were collected for RNA-seq library construction using Smart-Seq2 methods.

The reads were mapped to mm10 from the UCSC genome (http://genome.ucsc.edu/) via HISAT2 (v2.1.0) with default parameters [28]. The read counts of each gene annotated in Gencode vM17 were calculated via featureCounts with default parameters [29]. Sum factor normalization was applied with deconvolution of size factors within different batch samples via SCnorm. Raw counts were normalized by library size via TPM. DEGs between different groups were analyzed via limma (v.3.56.2). DEGs were defined as those whose log2-fold change was greater than the log2 (1.5) and whose adjusted p value was <0.05. GO enrichment analysis of the DEGs was performed via clusterProfiler (v.4.8.3). The results were visualized via ggplot2 (v.3.4.4). Gene set enrichment analysis was performed via clusterProfiler (v.4.8.3). Gene ontology gene sets were obtained from the Molecular Signatures Database (v.7.5.1). The results were visualized via GseaVis (v.0.8.8).

2.14 | Statistical Analysis

The data are presented as the means ± SEMs. Statistical analyses were performed via an unpaired two-tailed Student's t-test in PRISM software (GraphPad 8 Software) to compare the differences between the treatment and control groups, assuming equal variance. The Mann–Whitney test was used to determine the significance of differences between data without a normal distribution. One-way or two-way ANOVA with Tukey's test was used for multiple comparisons. The chi-square test was used to test differences between two groups for categorical variables. *, **, *** and **** indicate $p<0.05$, $p<0.01$, $p<0.001$ and $p<0.0001$, respectively. ns, not significant.

3 | Results

3.1 | Short-Term Rapamycin Treatment Alleviates Ovarian Aging Phenotypes

We reanalyzed transcriptome data from oocytes and granulosa cells (GCs, specifically cumulus cells) of 2-month-old and 10-month-old mice [30]. In oocytes from 10-month-old mice, upregulated differentially expressed genes (DEGs) were enriched in Gene Ontology (GO) terms related to cytoplasmic translation, ribosome biogenesis, and TOR signaling, as confirmed by gene set enrichment analysis (GSEA) (Figure 1A–C). Similarly, in GCs from 10-month-old mice, upregulated DEGs were linked to cytoplasmic translation, ribosome biogenesis, the humoral immune response, and complement activation (Figure 1D–F). Given the established role of mTOR in ribosome biogenesis, translation, and inflammation [31], we administered rapamycin (8.0 mg/kg/day) to 10-month-old female mice for 1 month (Figure 2A). While ovarian and body weights remained unaffected (Figure S1A,B), rapamycin significantly reduced phosphorylated S6 (p-S6) levels in ovarian tissue (Figure 2B,C) and downregulated ribosome-related genes (Rpl36, Rpl5) (Figure 2D), confirming effective suppression mTOR signaling. Furthermore, rapamycin treatment markedly reduced levels of SA-β-gal (Figure 2E), inflammatory factors (TNF-α and CXCL2, Figure S1C) and fibrosis markers in the ovary (Figure 2F,G, Figure S1C). It also attenuated the elevated p-S6 levels and inflammatory factor expression in GCs from reproductively aged mouse (Figure 2H,I), suggesting a beneficial effect of rapamycin on the ovarian somatic

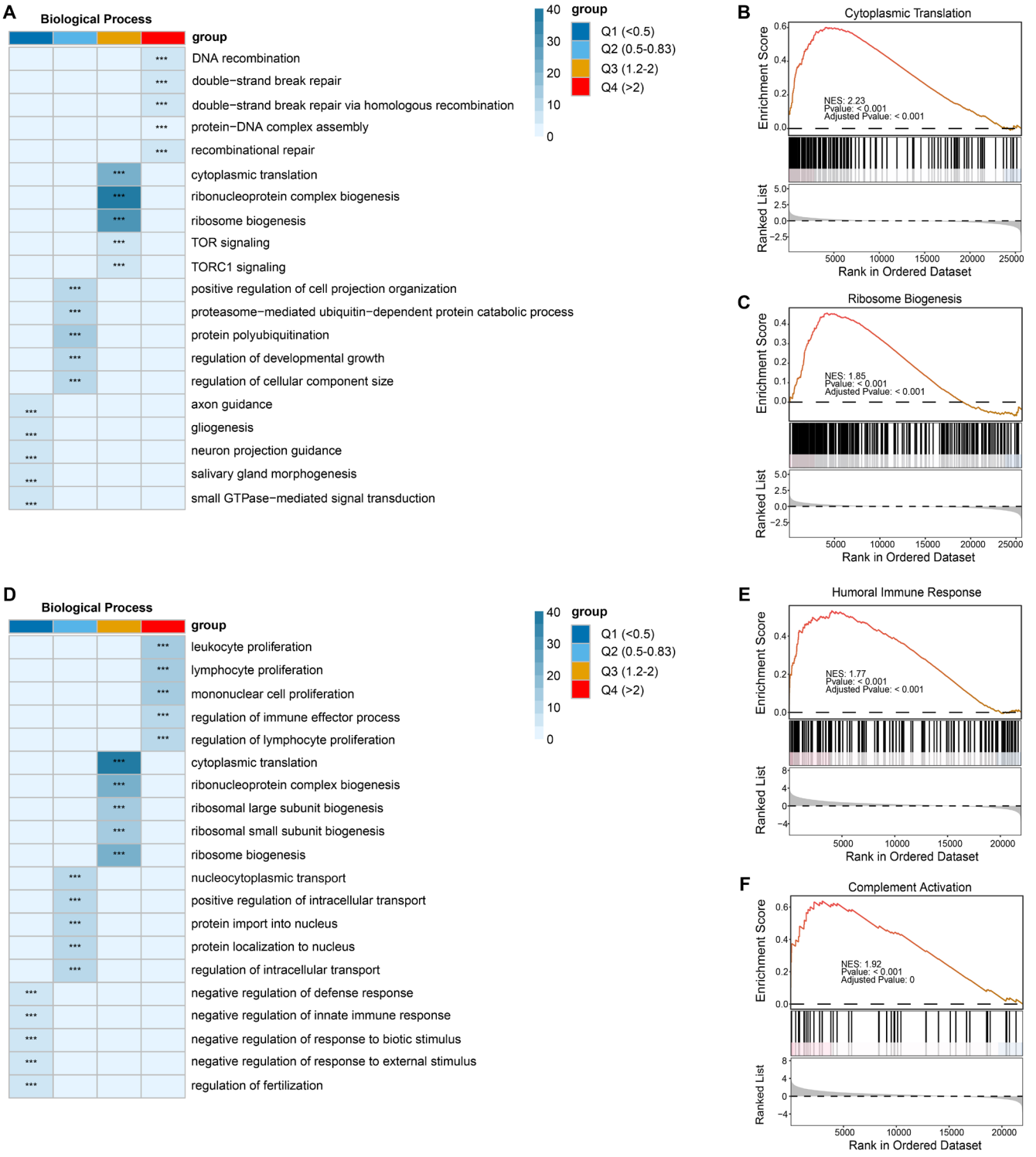

FIGURE 1 | Age-related transcriptome changes in oocytes and granulosa cells. (A) GO enrichment analysis of biological processes in young or old oocytes. (B) GSEA map showing upregulated cytoplasmic translation in old oocytes. (C) GSEA map showing upregulated ribosome biogenesis in old oocytes. (D) GO enrichment analysis of biological processes in young and old granulosa cells. (E) GSEA map showing an upregulated humoral immune response in old granulosa cells. (F) GSEA map showing upregulated complement activation in old granulosa cells.

microenvironment. However, mating experiments with young males showed that rapamycin did not improve fertility in these reproductively aged females, as evidenced by no significant increase in offspring number (Figure S1D). Moreover, the decline in serum estradiol (E2) levels, the primary circulating estrogen reflecting ovarian endocrine function, observed

in reproductively aged mice was not reversed by rapamycin treatment (Figure S1E). Thus, although short-term rapamycin treatment alleviates age-related ovarian alterations and improves the somatic environment, it does not restore reproductive function in reproductively aged mice.

3.2 | Short-Term Rapamycin Treatment Mitigates Age-Related Features in Somatic Organs

Given the observed beneficial effects of rapamycin on the ovarian somatic microenvironment, we next investigated whether

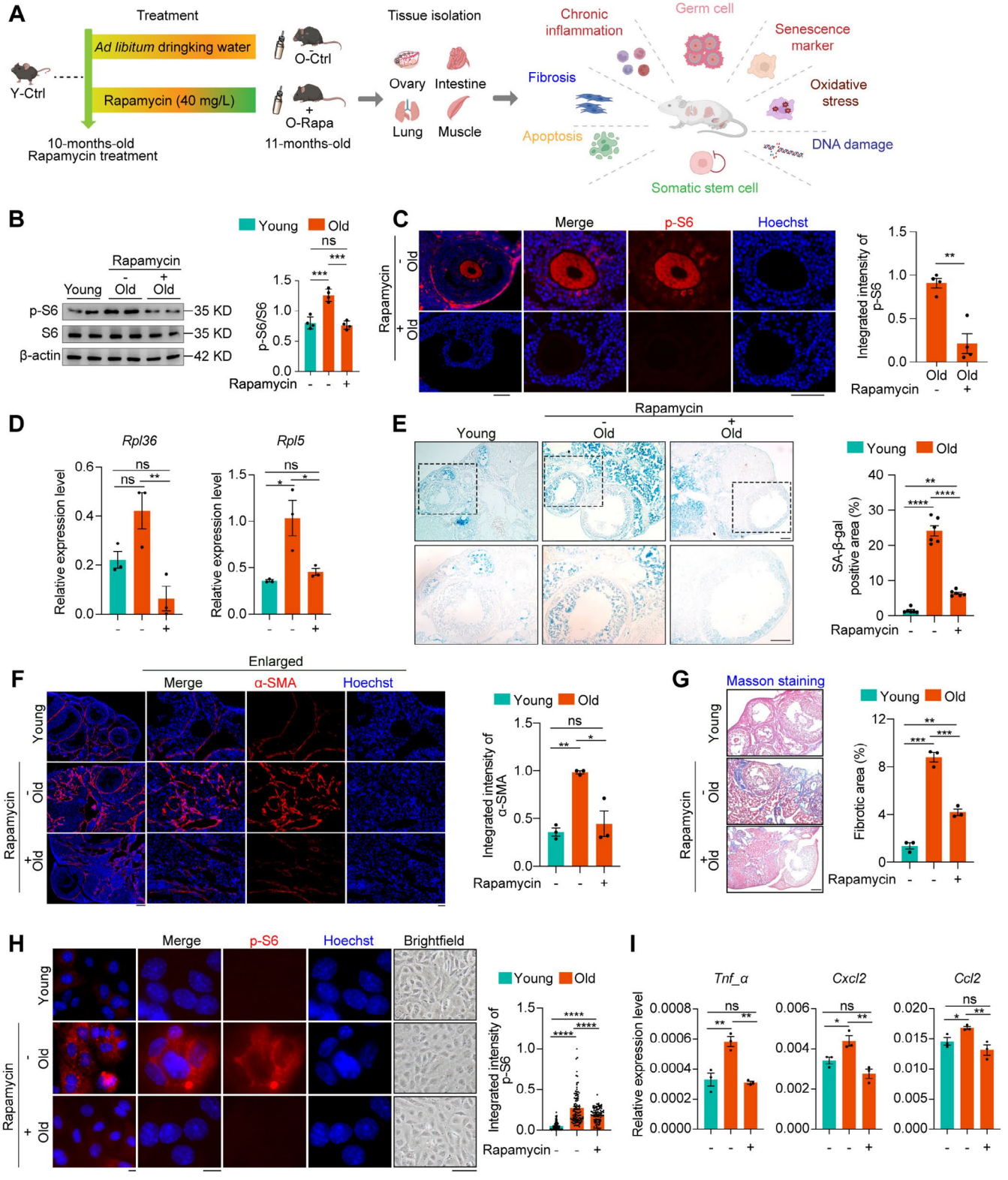

FIGURE 2 | Legend on next page.

FIGURE 2 | Short-term rapamycin delays ovarian tissue aging phenotypes. (A) Ten-month-old mice were administered either rapamycin (O-Rapa) or ad libitum drinking water (O-CTRL) for 1 month. Two-month-old mice receiving drinking water served as the young control (Y-CTRL). (B) Western blot analysis of phosphorylated S6 (p-S6) and total S6 protein levels in ovaries from young and reproductively aged mice treated with or without rapamycin for one month; β-actin was used as a loading control. Data are presented as the mean ± SEM, $n = 4$ mice per group. $^{**}p < 0.01$ (two-tailed unpaired t test). (C) Immunofluorescence of p-S6 in ovarian sections from reproductively aged mice with or without rapamycin treatment. Scale bar, 100 μm. Data are presented as the mean ± SEM, $n = 4$ mice per group. $^{**}p < 0.01$ (two-tailed unpaired t test). (D) qPCR analysis of ribosome-related genes (*Rpl36* and *Rpl5*) in ovaries from young and reproductively aged mice treated with/without rapamycin, normalized to *Gapdh*. (E) SA-β-gal staining of ovarian sections from young and reproductively aged mice treated with or without rapamycin (scale bar = 100 μm), with quantification of the SA-β-gal-positive area. The data are presented as the mean ± SEM, $n = 6$ mice per group. (F) Immunofluorescence of α-SMA and (G) Masson staining of ovarian sections from young and reproductively aged mice treated with or without rapamycin. Scale bar, 100 μm. Quantification of α-SMA fluorescence intensity and the fibrotic area is shown on the right. The data are presented as the mean ± SEM, $n = 3$ mice per group. (H) p-S6 immunofluorescence in GCs from young and reproductively aged mice treated with or without rapamycin. Scale bar, 10 μm. The quantification of the fluorescence intensity is shown on the right. The data are presented as the mean ± SEM, $n = 100$ cells. (I) qPCR analysis of inflammation-related factors in GCs from young and reproductively aged mice treated with or without rapamycin normalized to *Gapdh*. The data are presented as the mean ± SEM, $n = 3$ mice per group. ns, not significant, $^{*}p < 0.05$, $^{**}p < 0.01$, $^{***}p < 0.001$, $^{****}p < 0.0001$, ANOVA tests (multiple comparisons).

similar anti-aging benefits could be detected in non-reproductive somatic organs, especially the lung, small intestine, and skeletal muscle in reproductively aged mice. Ten-month-old female mice were treated with rapamycin for 1 month, with 2-month-old mice serving as young controls. Compared to reproductively aged mice provided ad libitum drinking water (O-CTRL), rapamycin-treated mice exhibited reduced phosphorylation of mTOR (Ser2448) and its downstream target S6 in lung, small intestine, and skeletal muscle tissues (Figure 3A,B, Figure S2A–C), confirming systemic inhibition of mTOR signaling. Histological analysis by H&E staining further revealed that rapamycin alleviated several age-related structural alterations, including changes in the morphology and number of small intestinal villi and crypts [32, 33], as well as reduced skeletal muscle fiber size (Figure 3C and Figure S2D). Consistently, rapamycin treatment also reduced the abundance of p16INK4A-positive senescent cells (Figure 3D, Figure S2A–C) and decreased apoptosis (Figure S2E) across these tissues. Together, these results indicate that short-term rapamycin treatment not only counteracts cellular senescence but also ameliorates aging-associated tissue degeneration in multiple somatic organs.

3.3 | Rapamycin Alleviates Tissue Inflammation, Fibrosis, and Oxidative Damage

Having established that rapamycin mitigates structural and cellular aging phenotypes in both somatic and ovarian tissues, we further investigated its effect on key molecular drivers of aging, including chronic inflammation, fibrosis, and oxidative stress. Senescent cells and their associated secretory phenotype (SASP) are major contributors to age-related chronic inflammation and immune dysregulation [34]. Moreover, rapamycin has been suggested to suppress inflammation and promote healthspan via S6K inhibition [35]. Consistent with this, cytokine analysis revealed that rapamycin significantly lowered the levels of multiple proinflammatory cytokines, including IFN-γ, TNF-α, IL-1β, CXCL1, and CCL5 in lung, small intestine, and skeletal muscle tissues (Figure 4A–C, Figure S2A–C). Immunohistochemical (IHC) staining and Western blot analysis further confirmed that rapamycin decreased TNF-α and IL-1β levels in the lung, small intestine, and skeletal muscle (Figure 4D,E, Figure S2A–C). In addition to attenuating inflammation, rapamycin treatment reduced oxidative stress, as indicated by decreased 8-OHdG staining (Figure 4F) and ameliorated fibrosis, evidenced by diminished α-SMA and Masson's trichrome staining in these tissues (Figure 4G, Figure S2A–C, Figure S2F). Collectively, these findings demonstrate that short-term rapamycin treatment alleviates multiple hallmarks of aging in somatic organs, including inflammation, oxidative damage, and fibrosis, thereby contributing to improved tissue homeostasis.

3.4 | Short-Term Rapamycin Treatment Reverses Somatic Stem Cell Exhaustion and Senescence in Reproducing Aged Mice

Building on the observed improvements in tissue homeostasis and attenuation of inflammatory and fibrotic changes, we sought to determine whether rapamycin could counteract stem cell exhaustion—a key hallmark of aging [36]. Given the central role of mTOR signaling in regulating stem cell self-renewal, differentiation, and stemness [37]. we hypothesized that rapamycin might restore stem cell function in reproductively aged mice. Indeed, although we confirmed a marked reduction in adult stem cell numbers across multiple tissues in reproductively aged mice, rapamycin treatment partially restored stem cell populations, as indicated by increased expression of PAX7, a marker of quiescent muscle stem cells (MuSCs), in skeletal muscle and LGR5, a well-established marker of intestinal stem cells located at the crypt base, in the small intestine (Figure 5A–C). Furthermore, rapamycin enhanced the expression of the proliferation marker PCNA in intestinal crypts as well as alveolar type 2 (AT2) cells (the resident progenitor cells responsible for alveolar regeneration), effectively countering age-related declines in proliferative capacity (Figure 5D,E). Aging is also characterized by the accumulation of DNA damage and elevated expression of senescence markers such as p16INK4A and γH2AX, which contribute to stem cell dysfunction [36, 38, 39]. Quantitative immunofluorescence analysis revealed a significant increase in $SPC^+/p16INK4A^+$ and $SPC^+/\gamma H2AX^+$ cells in the lungs of reproductively aged control mice compared to young controls. Rapamycin treatment, however, markedly reduced the number of these senescent stem cells (SPC^+/

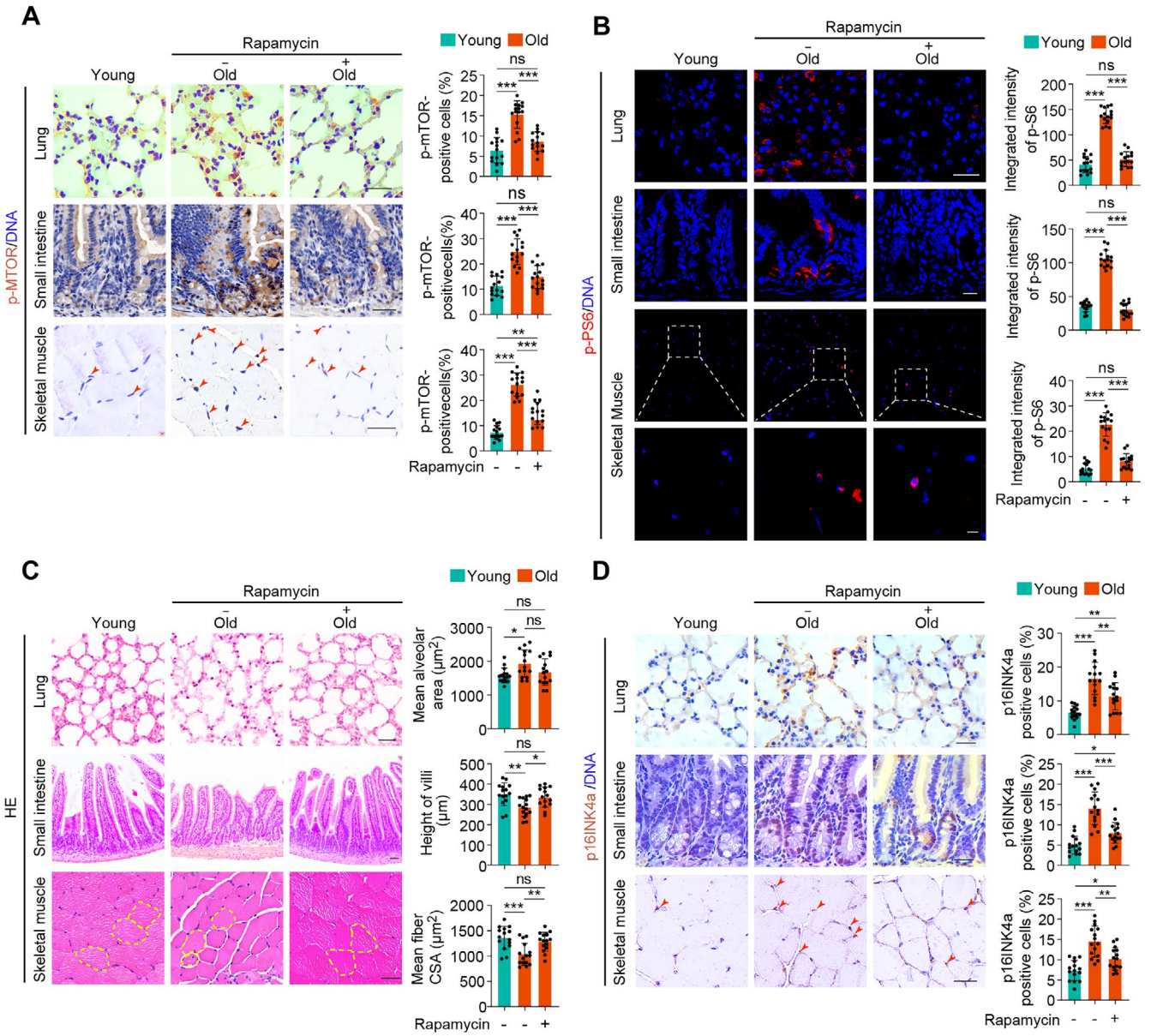

FIGURE 3 | Geroprotective effects of rapamycin on somatic tissue. (A) Immunohistochemical assessment of p-mTOR in the lung, small intestine, and muscle of young and reproductively aged mice treated with or without rapamycin. Scale bars: Lung and skeletal muscle, 25 μm; small intestine, 50 μm. (B) Immunofluorescence of p-S6 in the lung, small intestine, and skeletal muscle of young and reproductively aged mice treated with or without rapamycin. Scale bars: 25 μm. (C) H&E staining of lung, small intestine, and skeletal muscle from young and reproductively aged mice treated with or without rapamycin. Scale bars: Lung and skeletal muscle, 25 μm; small intestine, 50 μm. The yellow dotted lines outline skeletal muscle fibers. (D) Immunohistochemical assessment of p16INK4A in the lung, small intestine, and skeletal muscle of young and reproductively aged mice treated with or without rapamycin. Arrows indicate p16INK4A-positive cells. Scale bars: 50 μm. Representative images (left) and statistics (right) of young and reproductively aged mice treated with or without rapamycin in (B)–(D). The data are presented as the mean ± SEM, $n = 15$ regions per group (collected from three mice per group). ns, not significant, *$p < 0.05$, **$p < 0.01$, ***$p < 0.001$, ANOVA (multiple comparisons).

p16INK4A$^+$, SPC$^+$/γH2AX$^+$, and PAX7$^+$/p16INK4A$^+$) in lung tissue (Figure 6A–D). Similarly, rapamycin decreased PAX7$^+$/p16INK4A$^+$ double-positive cells and γH2AX-positive cells in skeletal muscle and small intestinal crypts (Figure 6A–D). Together, these data indicate that short-term rapamycin treatment not only mitigates tissue-level aging phenotypes but also rejuvenates somatic stem cells by alleviating senescence and DNA damage, thereby counteracting stem cell exhaustion in reproductively aged female mice.

3.5 | Rapamycin Restores Stem Cell Differentiation Potential

Given that rapamycin alleviates stem cell senescence and exhaustion, we further investigated its capacity to rescue age-related impairments in stem cell differentiation. In the lung, where AT2 cells function as primary progenitors capable of self-renewal and differentiation into AT1 cells [40], rapamycin promoted the differentiation of AT2 to AT1 cells, as shown by an increased

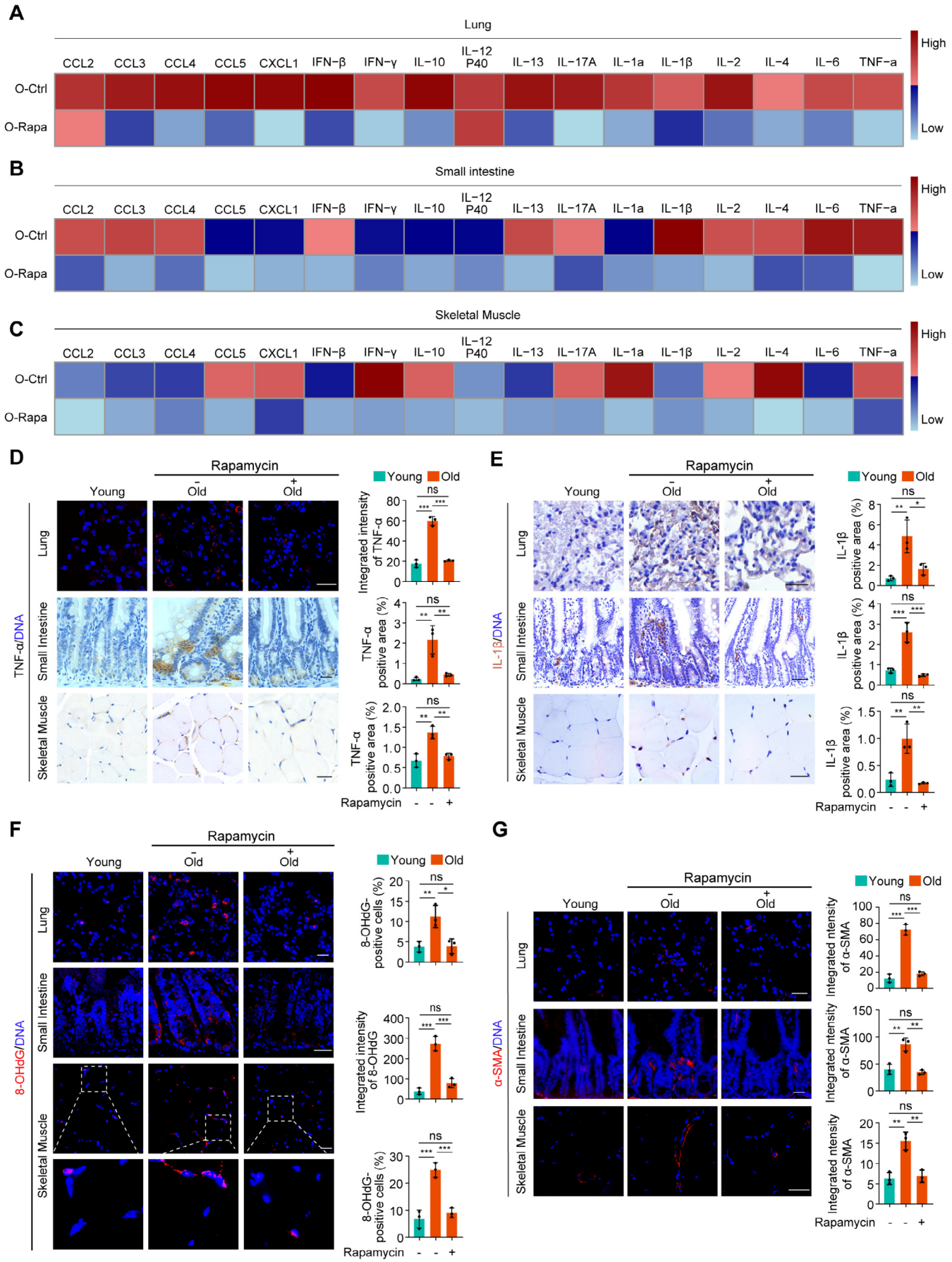

FIGURE 4 | Legend on next page.

FIGURE 4 | Rapamycin alleviates tissue inflammation, fibrosis, and oxidative damage. (A) Lung, small intestine (B) and (C) skeletal muscle tissues from reproductively aged mice treated with or without rapamycin were analyzed. A heatmap of inflammatory cytokine levels revealed variations across groups. The samples from the three groups of mice were pooled for testing (3 mice per group). Cytokines and chemokines in the mouse serum were detected via the ABplex Mouse Plex Custom Panel. (D) Immunofluorescence and immunohistochemistry of TNF-α in the lung, small intestine, and skeletal muscle of young and reproductively aged mice treated with or without rapamycin. Scale bars: 25 μm. (E) Immunohistochemical assessment of IL-1β in the lung, small intestine, and skeletal muscle of young and reproductively aged mice treated with or without rapamycin, with arrows indicating IL-1β-positive cells. Scale bars: Lung and skeletal muscle, 25 μm; small intestine, 50 μm. (F) Immunofluorescence of 8-OHdG in the lung, small intestine, and skeletal muscle. Scale bars: 25 μm. (G) Immunofluorescence of α-SMA in the lung, small intestine, and skeletal muscle. Scale bars: 25 μm. Representative images (left) and statistics (right) for young control and reproductively aged rapamycin-treated mice in (C)–(F). The data are expressed as the mean ± SEM ($n = 3$ mice per group). ns (not significant), $^{*}p < 0.05$; $^{**}p < 0.01$; $^{***}p < 0.001$; ANOVA (multiple comparisons).

number of HOPX^{+} AT1 cells (HOPX+: marker of differentiated alveolar type I cells) (Figure 7A). In the small intestine, aging skews intestinal stem cell (ISC) differentiation toward secretory lineages [41, 42]. Rapamycin counteracted this bias, reducing the age-associated expansion of Paneth cells (LYZ^{+}) and goblet cells (Alcian blue^{+}) and thereby improving ISC differentiation outcomes (Figure 7B,C). In skeletal muscle, where PAX7 marks quiescent MuSCs, aging shifts MuSCs toward precocious activation and differentiation [43–46]. Consistent with this, we observed fewer quiescent PAX7^{+} cells and more activated PAX7^{+}/MYOD^{+} cells in reproductively aged muscle (MYOD^{+}: indicator of activated myogenic differentiation). Rapamycin treatment restored the quiescent pool of PAX7^{+} MuSCs and reduced the proportion of PAX7^{+}/MYOD^{+} activated cells (Figure 7D). Taken together, these results indicate that rapamycin not only preserves stem cell numbers and reduces senescence but also reinstates their functional differentiation capacity across multiple tissues in reproductively aged mice.

3.6 | Reversible Effects of Short-Term Rapamycin Treatment After Withdrawal

Given the improvements in stem cell function and tissue homeostasis induced by rapamycin, we sought to determine whether these benefits persist after treatment cessation. Since anti-aging interventions often exhibit transient effects that may reverse upon withdrawal [13], and considering that rapamycin injection at 8 mg/kg/day for 3 months does not increase the life expectancy of female mice starting at 20–21 months of age [47], we then evaluated the sustainability of rapamycin-mediated benefits following a one-month withdrawal period (OLD^{RW}) after initial treatment (Figure S3A). After rapamycin withdrawal, the suppression of mTOR signaling was no longer maintained. p-mTOR and p-S6 levels in lung, small intestine, and skeletal muscle reverted to those observed in age-matched 12-month-old controls (OLD^{12M}) (Figure S3B,C). Consistent with this molecular reversal, stem cell populations also regressed: the numbers of PAX7^{+} and LGR5^{+} stem cells in OLD^{RW} mice declined to minimal levels comparable to untreated reproductively aged controls (Figure S4A–C). Immunofluorescence analysis of PCNA and tissue-specific stem cells revealed only modest, non-significant increases in SPC^{+}/PCNA^{+} and PCNA^{+} cells in lung and intestinal tissues compared to OLD^{12M} mice (Figure S4D,E). Furthermore, the restored differentiation capacity observed during treatment was largely abolished after withdrawal, as shown by the loss of AT1 cell (HOPX^{+}) gains and the re-expansion of Paneth cells (Figure S5A,B). These data indicate that while short-term rapamycin treatment robustly improves somatic tissue integrity and stem cell function, its effects are largely reversible upon discontinuation. The anti-aging benefits—including mTOR pathway suppression, stem cell maintenance, and functional differentiation—diminish after treatment withdrawal, underscoring the necessity of sustained intervention for long-term tissue rejuvenation.

4 | Discussion

Our study demonstrates that short-term rapamycin treatment during the reproductive aging period in female mice effectively alleviates aging phenotypes across both reproductive and somatic tissues through mTOR pathway inhibition. These findings extend previous work on rapamycin's lifespan-extending properties to the context of perimenopausal aging. The multifaceted benefits observed, including delayed ovarian aging, reduced inflammation and fibrosis, and rejuvenated stem cell function, highlight rapamycin's potential in counteracting systemic aging processes. However, the failure to restore reproductive function and the reversible nature of these benefits upon treatment withdrawal reveal important limitations and tissue-specific considerations for clinical translation.

In the context of ovarian aging, our transcriptomic analyses revealed upregulated cytoplasmic translation and ribosome biogenesis pathways in both oocytes and GCs from reproductively aged mice, consistent with hyperactive mTOR signaling. Rapamycin effectively suppressed this pathway, as evidenced by reduced p-S6 levels and ribosome-related gene expression, subsequently attenuating senescence, fibrosis, and inflammation in the ovarian somatic microenvironment. However, despite these improvements at the molecular and cellular levels, rapamycin failed to restore fertility in reproductively aged females. This contrasts with earlier studies reporting that rapamycin preserves the follicle pool and extends ovarian lifespan in young/middle-aged females [10, 48–50]. Therefore, our findings suggest a fundamental age-related constraint: while rapamycin can modify the somatic environment, it cannot rescue fertility once advanced reproductive aging is established. Thus, the efficacy of mTOR inhibition appears critically dependent on intervention timing, with early treatment potentially sustaining the ovarian reserve while late intervention primarily ameliorates somatic dysfunction without restoring reproductive capacity.

Beyond the reproductive system, rapamycin demonstrated broad efficacy in mitigating age-related decline across somatic tissues.

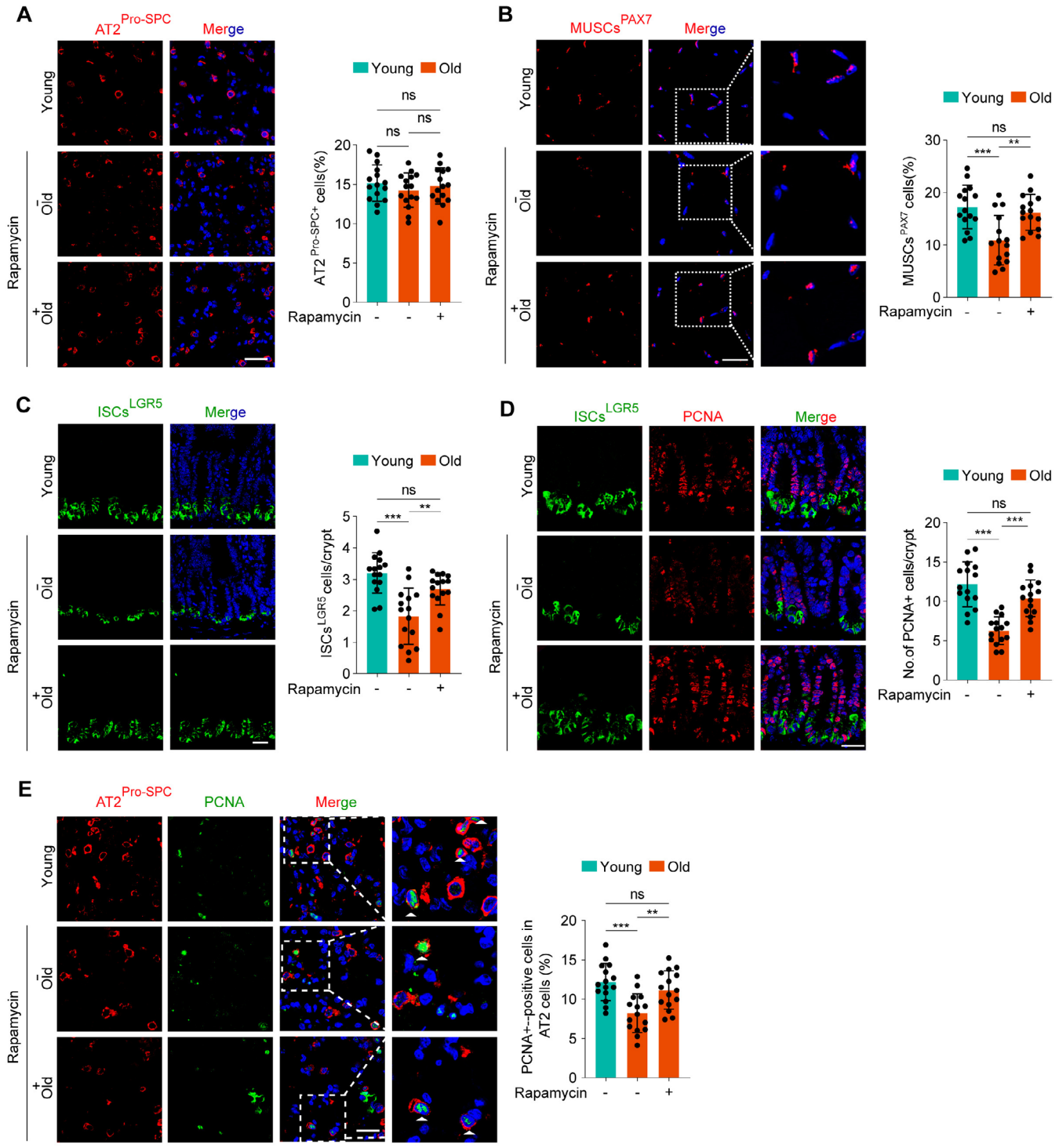

FIGURE 5 | Rapamycin promotes stem cell number and functions in multiple organs. (A–C) Representative images of (A) AT2$^{pro\text{-}SPC}$ (red), (B) MUSCs^{PAX7} (red), and (C) ISC^{LGR5} (green) immunostaining in the lungs, skeletal muscles, and small intestines of young and reproductively aged mice treated with or without rapamycin. Scale bars: 25 μm. (D-E) Quantification of (D) AT2$^{pro\text{-}SPC}$-PCNA-positive and (E) Crypt-PCNA-positive cells. (White arrowheads indicate double AT2$^{pro\text{-}SPC}$-PCNA-positive cells.) Scale bars for the lung and small intestine: 25 μm. Five random alveolar areas, muscle fibers, or crypts were quantified. The data are presented as the mean ± SEM, $n = 15$ regions per group (collected from three mice per group). ns, not significant, $^{**}p < 0.01$, $^{***}p < 0.001$, ANOVA (multiple comparisons).

The systemic inhibition of mTOR signaling was associated with structural improvements in lung, small intestine, and skeletal muscle, along with reduced cellular senescence and apoptosis. Importantly, rapamycin reversed stem cell exhaustion by restoring stem cell populations and proliferation capacity across multiple tissues. The enhanced differentiation potential observed in lung AT2 cells, intestinal stem cells, and muscle stem cells aligns with the conserved role of mTOR in regulating stem cell fate decisions [40–42]. These benefits extended to molecular hallmarks of aging, including reduced inflammation, oxidative

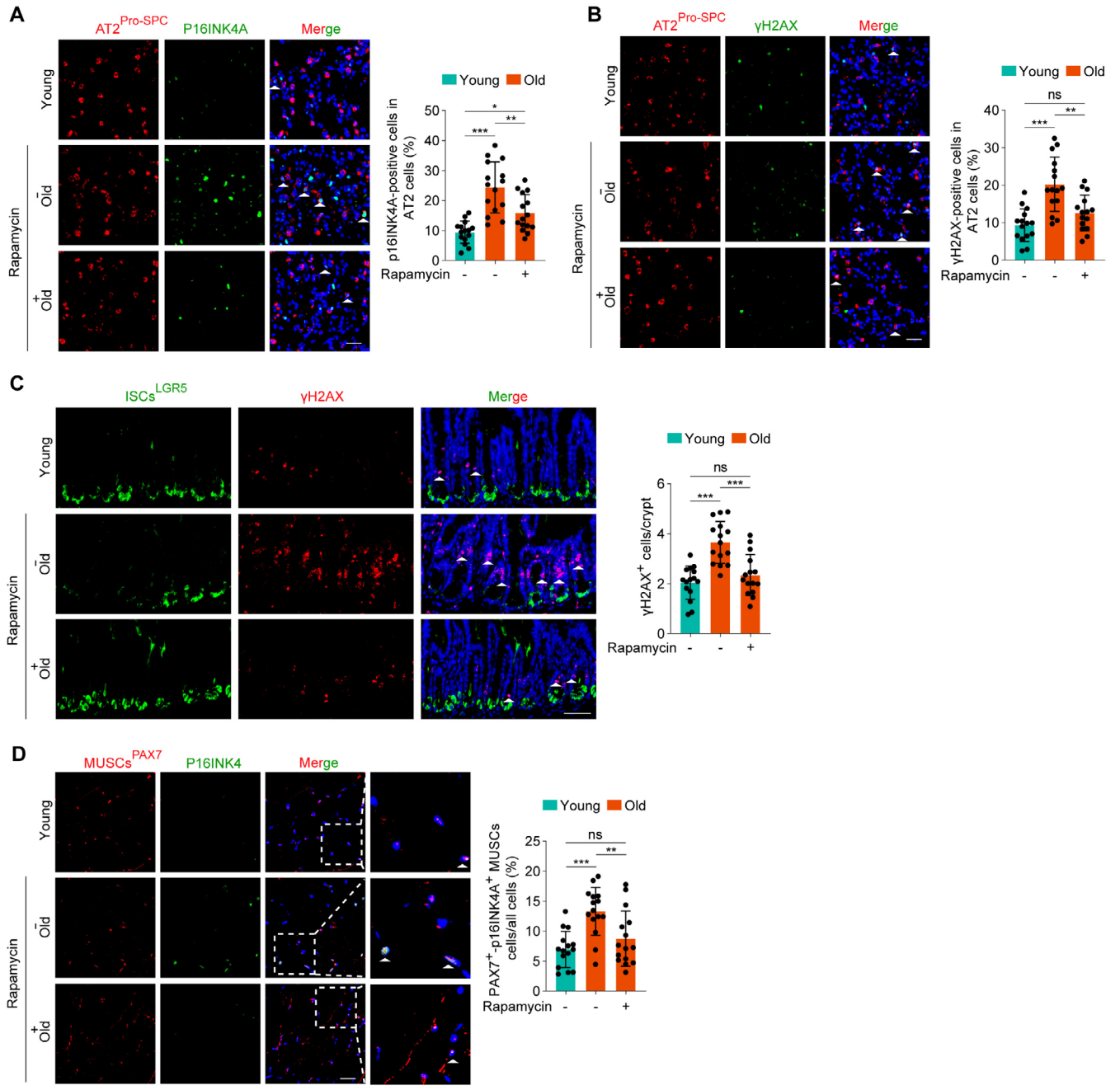

FIGURE 6 | Rapamycin mitigated stem cell senescence and reversed the increase in senescence-associated markers in AT2, Crypt, and MUSCs in the lungs, small intestines, and skeletal muscles of the mice. (A-B) Representative images of $AT2^{pro\text{-}SPC}$ (red), p16INK4A (green), and γH2AX (green) immunostaining in the lungs of young and reproductively aged mice, with quantification of (A) p16INK4A-positive $AT2^{pro\text{-}SPC}$ cells and (B) γH2AX-positive $AT2^{pro\text{-}SPC}$ cells. Scale bars: 25 μm. (C) Representative images of $ISCs^{LGR5}$ (green) and γH2AX (red) in the small intestines, with quantification of γH2AX-positive Crypt cells. Scale bars: 50 μm. (D) Representative images of $MUSCs^{PAX7}$ (red) and p16INK4A (green) immunostaining in skeletal muscle, with quantification of $PAX7^+/p16INK4A^+$ cells among all the cells. Scale bars: 25 μm. The data are presented as the mean ± SEM, $n = 15$ regions per group (collected from 3 mice per group). ns, not significant, $^*p < 0.05$, $^{**}p < 0.01$, $^{***}p < 0.001$, ANOVA (multiple comparisons).

stress, and fibrosis, collectively contributing to improved tissue homeostasis in reproductively aged females.

However, the benefits of short-term rapamycin treatment proved transient upon treatment cessation. The rapid reversal of mTOR suppression and the subsequent decline in stem cell function following drug withdrawal highlight the dependency of these anti-aging effects on sustained pathway inhibition. These findings align with studies in model organisms where rapamycin's benefits diminish after treatment discontinuation [13, 51] and raise important questions about optimal dosing regimens for long-term tissue rejuvenation. The observed reversibility, combined with evidence that late-life rapamycin initiation may not extend lifespan in female mice [47], suggests the existence of critical windows for intervention that vary across tissue types and functional outcomes.

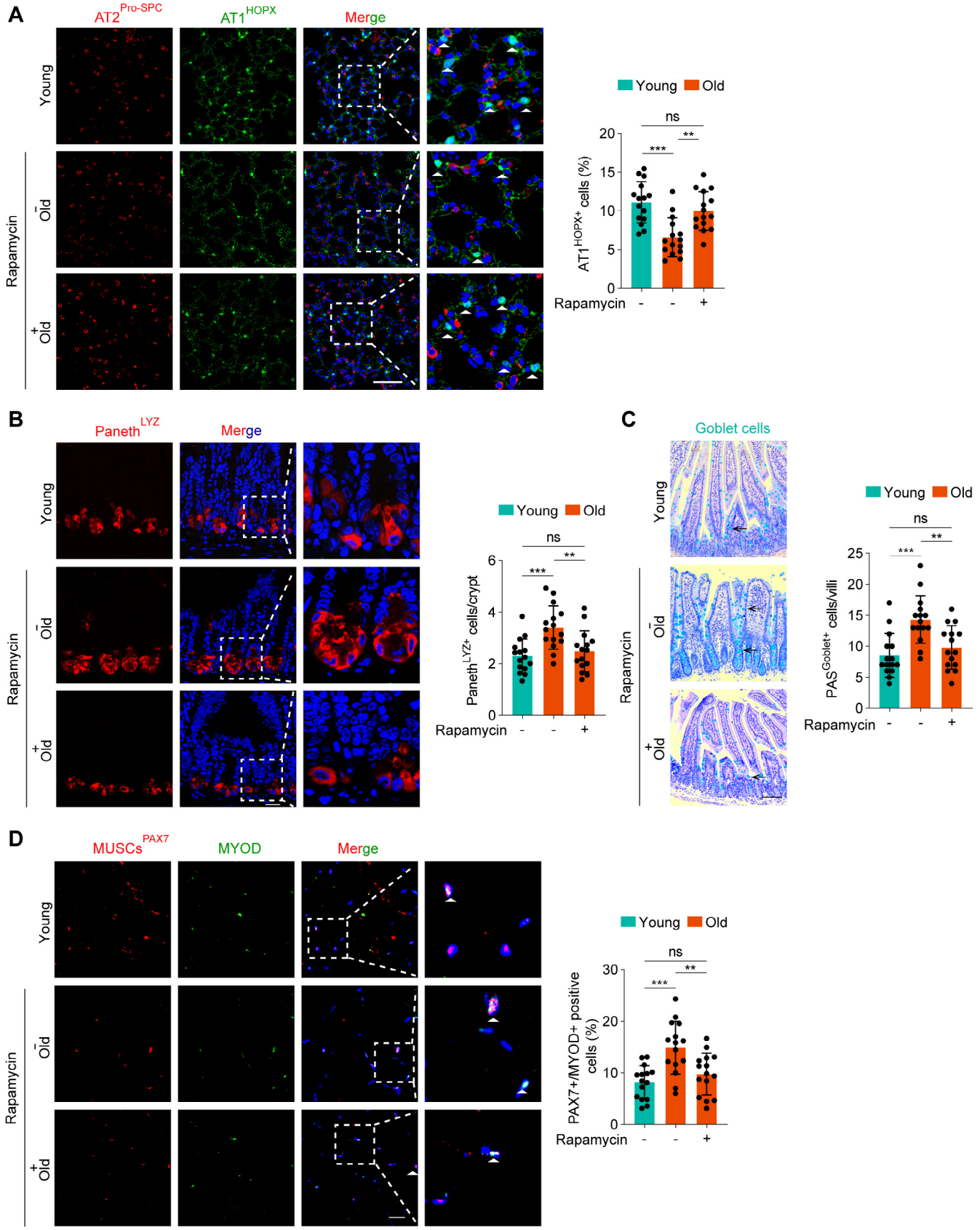

FIGURE 7 | Legend on next page.

In conclusion, our findings demonstrate that short-term rapamycin treatment differentially modulates tissue aging trajectories through mTOR inhibition. While effectively rejuvenating somatic stem cells and mitigating multiple hallmarks of aging across various organs, it fails to rescue reproductive function once advanced germ cell depletion has occurred. The reversible

FIGURE 7 | Rapamycin promotes the differentiation capacity of stem cells. (A) Representative images of $AT2^{pro\text{-}SPC}$ (red) and $AT1^{HOPX}$ (green) immunostaining in the lungs of young and reproductively aged mice, with quantification of $AT1^{HOPX}$-positive cells. The white arrowheads indicate $AT1^{HOPX}$-positive cells. Scale bars, 10 μm. (B-C) Representative immunostaining and AB-PAS images of (B) $Paneth^{LYZ}$ (red) and (C) goblet cells in the small intestines, with quantification of $Paneth^{LYZ}$-positive and goblet cells. The black arrowheads indicate goblet cells. Scale bars: $Paneth^{LYZ}$, 25 μm. goblet cells, 50 μm. (D) Representative images of $MUSCs^{PAX7}$ (red) and MYOD (green) immunostaining in skeletal muscle, with quantification of $PAX7^{+}/MYOD^{+}$ positive cells. Scale bars, 25 μm. The white arrowheads indicate $PAX7^{+}/MYOD^{+}$ positive cells. Five random alveolar areas, muscle fibers or crypts were quantified. The data are presented as the mean ± SEM, $n = 15$ regions per group (collected from 3 mice per group). ns (not significant), $^{**}p < 0.01$, $^{***}p < 0.001$, ANOVA (multiple comparisons).

nature of these benefits upon treatment withdrawal underscores the need for continued investigation into optimal treatment timing, duration, and potential combination therapies. Future studies should explore whether intermittent dosing regimens or earlier intervention strategies could maximize rapamycin's anti-aging benefits while minimizing potential side effects, particularly in the context of female reproductive aging and associated systemic decline.

Author Contributions

Jiangtao Lu: data curation, formal analysis, investigation, methodology, visualization, writing – original draft, writing – review and editing. **Jie Li:** data curation, investigation, software, writing – original draft, methodology, validation. **Chang Liu:** investigation, methodology. **Guofeng Feng:** investigation, methodology. **Guoxing Yin:** software, methodology. **Ziyue Hu:** data curation, methodology. **Dai Heng:** investigation, methodology. **Yongqin Yu:** investigation, methodology. **Kairang Jin:** methodology. **Yiwei Wu:** methodology. **Zhuangzhuang Feng:** software. **Junru Chen:** software. **Yufei Wei:** methodology. **Yating Wang:** methodology. **Xuemin Hu:** visualization. **Lin Liu:** conceptualization, investigation, funding acquisition, project administration, resources, supervision, validation, writing – review and editing. **Xue Du:** conceptualization, visualization, investigation, supervision, funding acquisition, project administration. **Zhengmao Zhu:** conceptualization, data curation, investigation, project administration, supervision, validation, writing – review and editing.

Funding

This study was supported by The National Key Research and Development Program of China 2022YFA1103800; General Program of Tianjin Bureau of Science and Technology 22JCYBJC00710, 23JCZDJC00820.

Conflicts of Interest

The authors declare no conflicts of interest.

Data Availability Statement

Mouse oocyte and GC RNA-seq data were downloaded from our previous publication (GSE184637) [30]. No original code is featured in this paper. Any additional information required to reanalyze the data reported in this paper is available from the lead contact upon request.

References

1. X. T. Shen, C. C. Wang, X. Zhou, et al., "Nonlinear Dynamics of Multi-Omics Profiles During Human Aging," *Nature Aging* 4 (2024): 1619–1634.

2. K. Abe, H. Ino, T. Niwa, et al., "Sex-Dependent Regulation of Vertebrate Somatic Growth and Aging by Germ Cells," *Science Advances* 10, no. 24 (2024): eadi1621.

3. M. Wu, W. C. Tang, Y. Chen, et al., "Spatiotemporal Transcriptomic Changes of Human Ovarian Aging and the Regulatory Role of FOXP1," *Nature Aging* 4, no. 4 (2024): 527–545.

4. T. L. King, K. B. Underwood, K. K. Hansen, et al., "Chronological and Reproductive Aging-Associated Changes in Resistance to Oxidative Stress in Post-Reproductive Female Mice," *Geroscience* 46, no. 1 (2023): 1159–1173.

5. J. A. Loose, F. R. G. Amrit, T. Patil, J. L. Yanowitz, and A. Ghazi, "Meiotic Dysfunction Accelerates Somatic Aging in Caenorhabditis Elegan," *Aging Cell* 21, no. 11 (2022): e13716.

6. N. Maharajan, K. Vijayakumar, C. H. Jang, and G. W. Cho, "Caloric Restriction Maintains Stem Cells Through Niche and Regulates Stem Cell Aging," *Journal of Molecular Medicine* 98, no. 1 (2020): 25–37.

7. S. Haller, S. Kapuria, R. R. Riley, et al., "mTORC1 Activation During Repeated Regeneration Impairs Somatic Stem Cell Maintenance," *Cell Stem Cell* 21, no. 6 (2017): 806–818.e5.

8. Y. S. Cai, W. Song, J. M. Li, et al., "The Landscape of Aging," *Science China. Life Sciences* 65, no. 12 (2022): 2354–2454.

9. A. Di Francesco, A. G. Deighan, L. Litichevskiy, et al., "Dietary Restriction Impacts Health and Lifespan of Genetically Diverse Mice," *Nature* 634, no. 8034 (2024): 684–692.

10. X. W. Dou, Y. Sun, J. Z. Li, et al., "Short-Term Rapamycin Treatment Increases Ovarian Lifespan in Young and Middle-Aged Female Mice," *Aging Cell* 16, no. 4 (2017): 825–836.

11. L. Fontana, L. Partridge, and V. D. Longo, "Extending Healthy Life Span-From Yeast to Humans," *Science* 328, no. 5976 (2010): 321–326.

12. D. N. Garcia, T. D. Saccon, J. Pradiee, et al., "Effect of Caloric Restriction and Rapamycin on Ovarian Aging in Mice," *Geroscience* 41, no. 4 (2019): 395–408.

13. A. V. Shindyapina, Y. M. Cho, A. Kaya, et al., "Rapamycin Treatment During Development Extends Life Span and Health Span of Male Mice and Daphnia Magna," *Science Advances* 8, no. 37 (2022): eabo5482.

14. T. L. Kaeberlein, A. S. Green, G. Haddad, et al., "Evaluation of Off-Label Rapamycin Use to Promote Healthspan in 333 Adults," *Geroscience* 45, no. 5 (2023): 2757–2768.

15. D. J. W. Lee, A. H. Kuerec, and A. B. Maier, "Targeting Ageing With Rapamycin and Its Derivatives in Humans: A Systematic Review," *Lancet Healthy Longevity* 5, no. 2 (2024): e152–e162.

16. J. Li, M. Xiong, X. H. Fu, et al., "Determining a Multimodal Aging Clock in a Cohort of Chinese Women," *Medicus* 4, no. 11 (2023): 825–848.

17. A. Houssaini, M. Breau, K. Kebe, et al., "mTOR Pathway Activation Drives Lung Cell Senescence and Emphysema," *JCI Insight* 3, no. 3 (2018): e93203.

18. R. Babaei-Jadidi, D. Clements, Y. Wu, et al., "mTOR Dysregulation Induces IL-6 and Paracrine AT2 Cell Senescence Impeding Lung Repair in Lymphangioleiomyomatosis," *Nature Communications* 16, no. 1 (2025): 8996.

19. D. He, H. Wu, J. Xiang, et al., "Gut Stem Cell Aging Is Driven by mTORC1 via a p38 MAPK-p53 Pathway," *Nature Communications* 11, no. 1 (2020): 37.

20. C. K. Kikani, X. Wu, S. Fogarty, et al., "Activation of PASK by mTORC1 Is Required for the Onset of the Terminal Differentiation Program," *Proceedings of the National Academy of Sciences of the United States of America* 116, no. 21 (2019): 10382–10391.

21. T. L. Habermehl, K. B. Underwood, K. D. Welch, et al., "Aging-Associated Changes in Motor Function Are Ovarian Somatic Tissue-Dependent, but Germ Cell and Estradiol Independent in Post-Reproductive Female Mice Exposed to Young Ovarian Tissue," *Geroscience* 44, no. 4 (2022): 2157–2169.

22. D. Heng, X. Y. Sheng, C. L. Tian, et al., "Mtor Inhibition by INK128 Extends Functions of the Ovary Reconstituted From Germline Stem Cells in Aging and Premature Aging Mice," *Aging Cell* 20, no. 2 (2021): e13304.

23. J. Li, H. Wang, P. Zhu, et al., "Ribosome Dysregulation and Intervention in Age-Related Infertility," *Cell Reports Medicine* 6, no. 11 (2025): 102424.

24. X. Deng, X. Zhang, W. P. Li, et al., "Chronic Liver Injury Induces Conversion of Biliary Epithelial Cells Into Hepatocytes," *Cell Stem Cell* 23, no. 1 (2018): 114–122.e3.

25. J. Mao and L. Liu, "Generation of iPS Cells From Granulosa Cells," *Methods in Molecular Biology* 1357 (2016): 451–464.

26. C. Tian, L. Liu, X. Ye, et al., "Functional Oocytes Derived From Granulosa Cells," *Cell Reports* 29, no. 13 (2019): 4256–4267.e9.

27. X. Zhang, H. Xu, J. Z. Yu, et al., "Immune Regulation of the Liver Through the PCSK9/CD36 Pathway During Heart Transplant Rejection," *Circulation* 148, no. 4 (2023): 336–353.

28. D. Kim, B. Langmead, and S. L. Salzberg, "HISAT: A Fast Spliced Aligner With Low Memory Requirements," *Nature Methods* 12, no. 4 (2015): 357–360.

29. Y. Liao, G. K. Smyth, and W. Shi, "featureCounts: An Efficient General Purpose Program for Assigning Sequence Reads to Genomic Features," *Bioinformatics* 30, no. 7 (2014): 923–930.

30. M. Gou, J. Li, L. Yi, et al., "Reprogramming of Ovarian Aging Epigenome by Resveratrol," *PNAS Nexus* 2, no. 2 (2023): pgac310.

31. J. B. Mannick and D. W. Lamming, "Targeting the Biology of Aging With mTOR Inhibitors," *Nature Aging* 3, no. 6 (2023): 642–660.

32. K. Nalapareddy, K. J. Nattamai, R. S. Kumar, et al., "Canonical Wnt Signaling Ameliorates Aging of Intestinal Stem Cells," *Cell Reports* 18, no. 11 (2017): 2608–2621.

33. L. Yang, Z. Ruan, X. Lin, et al., "NAD(+) Dependent UPR(Mt) Activation Underlies Intestinal Aging Caused by Mitochondrial DNA Mutations," *Nature Communications* 15, no. 1 (2024): 546.

34. V. Suryadevara, A. D. Hudgins, A. Rajesh, et al., "SenNet Recommendations for Detecting Senescent Cells in Different Tissues," *Nature Reviews Molecular Cell Biology* 25 (2024): 1001–1023.

35. S. Gallage, E. E. Irvine, J. E. B. Avila, et al., "Ribosomal S6 Kinase 1 Regulates Inflammaging via the Senescence Secretome," *Nature Aging* (2024): 1544–1561.

36. A. Brunet, M. A. Goodell, and T. A. Rando, "Ageing and Rejuvenation of Tissue Stem Cells and Their Niches," *Nature Reviews Molecular Cell Biology* 24, no. 1 (2023): 45–62.

37. H. N. Bao, J. N. Cao, M. T. Chen, et al., "Biomarkers of Aging," *Science China. Life Sciences* (2023): 893–1066.

38. M. Moqri, C. Herzog, J. Justice, et al., "Biomarkers of Aging for the Identification and Evaluation of Longevity Interventions," *Cell* 186, no. 18 (2023): 3758–3775.

39. J. Beumer and H. Clevers, "Hallmarks of Stemness in Mammalian Tissues," *Cell Stem Cell* 31, no. 1 (2024): 7–24.

40. K. Liu, X. F. Meng, Z. X. Liu, et al., "Tracing the Origin of Alveolar Stem Cells in Lung Repair and Regeneration," *Cell* 187, no. 10 (2024): 2428–2445.e20.

41. S. N. Liang, X. K. Guo, J. Y. Ou, et al., "Nutrient Sensing by the Intestinal Epithelium Orchestrates Mucosal Antimicrobial Defense via Translational Control of Hes1," *Cell Host & Microbe* 25, no. 5 (2019): 706–718.e7.

42. T. Jardé, C. M. Nefzger, J. M. Polo, and H. E. Abud, "Aging of Intestinal Stem Cells and Associated Niche," in *The Stem Cell Niche During Ageing* (Elsevier, 2020), 25–40.

43. S. Fukada and N. Ito, "Regulation of Muscle Hypertrophy: Involvement of the Akt-Independent Pathway and Satellite Cells in Muscle Hypertrophy," *Experimental Cell Research* 409, no. 2 (2021): 112907.

44. H. B. Zhang, D. Ryu, Y. B. Wu, et al., "NAD+ Repletion Improves Mitochondrial and Stem Cell Function and Enhances Life Span in Mice," *Science* 352, no. 6292 (2016): 1436–1443.

45. H. Li, Q. Chen, C. Y. Li, et al., "Muscle-Secreted Granulocyte Colony-Stimulating Factor Functions as Metabolic Niche Factor Ameliorating Loss of Muscle Stem Cells in Aged Mice," *EMBO Journal* 38, no. 24 (2019): e102154.

46. J. D. Bernet, J. D. Doles, J. K. Hall, K. K. Tanaka, T. A. Carter, and B. B. Olwin, "p38 MAPK Signaling Underlies a Cell-Autonomous Loss of Stem Cell Self-Renewal in Skeletal Muscle of Aged Mice," *Nature Medicine* 20, no. 3 (2014): 265–271.

47. A. Bitto, T. K. Ito, V. V. Pineda, et al., "Transient Rapamycin Treatment Can Increase Lifespan and Healthspan in Middle-Aged Mice," *eLife* 5 (2016): e16351.

48. X. Y. Chen, Z. J. Tang, H. Y. Guan, et al., "Rapamycin Maintains the Primordial Follicle Pool and Protects Ovarian Reserve Against Cyclophosphamide-Induced Damage," *Journal of Reproduction and Development* 68, no. 4 (2022): 287–294.

49. L. Y. Zhou, Y. Q. Xie, S. Li, et al., "Rapamycin Prevents Cyclophosphamide-Induced Over-Activation of Primordial Follicle Pool Through PI3K/Akt/mTOR Signaling Pathway in Vivo," *Journal of Ovarian Research* 10 (2017): 56.

50. X. M. Zhang, L. Li, J. J. Xu, et al., "Rapamycin Preserves the Follicle Pool Reserve and Prolongs the Ovarian Lifespan of Female Rats via Modulating mTOR Activation and Sirtuin Expression," *Gene* 523, no. 1 (2013): 82–87.

51. P. Juricic, Y. X. Lu, T. Leech, et al., "Long-Lasting Geroprotection From Brief Rapamycin Treatment in Early Adulthood by Persistently Increased Intestinal Autophagy," *Nature Aging* 2, no. 9 (2022): 824–836.

Supporting Information

Additional supporting information can be found online in the Supporting Information section. **FIGURE S1:** Effects of rapamycin on body weight and ovary weight in mice. Ovary shape, weight and (B) Body weight of young and aged mice treated with or without rapamycin for1 month ($n = 10$). (C) Western blot analysis of α-SMA, TNF-α and CXCL2 in ovaries from old mice treated with or without rapamycin for 1 month, with β-actin as a loading control. ($n = 3$ mice per group). (D) The numbers of pups from old mice treated with or without rapamycin were recorded and compared ($n = 8$ mice per group), the data are presented as the means ± SEMs. $^{**}p < 0.01$ unpaired Student's t test. (E) Serum estradiol (E2) levels of mice from young and aged mice treated with or without rapamycin ($n = 4$ mice per group). The data are presented as the means ± SEMs. ns, not significant, $^{*}p < 0.05$, $^{**}p < 0.01$, $^{***}p < 0.001$, $^{****}p < 0.0001$; ANOVA (multiple comparisons). **FIGURE S2:** Rapamycin treatment alleviates tissue apoptosis and fibrosis. (A) Western blot analysis of α-SMA, IL-1β, S6, p-S6, TNF-α, p16 in small

intestine from old mice treated with or without rapamycin for 1 month, with β-actin as a loading control. Samples from three mice per group were collected, with quantification shown on the right. (B) Western blot analysis of α-SMA, IL-1β, S6, p-S6, p16 in skeletal muscle from old mice treated with or without rapamycin for 1 month, with β-actin as a loading control. Samples from three mice per group were collected, with quantification shown on the right. (C) Western blot analysis of α-SMA, IL-1β, S6, p-S6, TNF-α, p16 in Lung from old mice treated with or without rapamycin for 1 month, with β-actin as a loading control, with quantification shown on the right. Samples from three mice per group were collected. (D) Representative TUNEL staining of the intestine and muscle from young and aged mice with or without rapamycin treatment, with quantification of TUNEL-positive cells shown on the right. Scale bars: small intestine, 75 μm; skeletal muscle, 25 μm. (E) Representative Masson staining of the lung, small intestine and skeletal muscle of young and aged mice treated with or without rapamycin, with quantification of the fibrotic area on the right. Scale bars: lung and skeletal muscle, 25 μm; small intestine, 50 μm. (F) The villus length and number of crypts per millimeter of small intestine are quantified, Related to Figure 3C = 15 regions per group (collected from 3 mice per group). The data are presented as the means ± SEMs. ns, not significant, $*p < 0.05$, $**p < 0.01$, $***p < 0.001$; ANOVA (multiple comparisons). **FIGURE S3:** Effect of rapamycin withdrawal on p-mTOR and p-S6 levels. (A) Schematic of rapamycin withdrawal analysis after 1 month of in vivo treatment. Following 1 month of treatment with either free water (O-CTRL) or rapamycin (O-Rapa), the OLD^{RW} group had rapamycin withdrawn and replaced with ad libitum drinking water for 1 month. The 12-month-old (OLD^{12M}) group with ad libitum access to water served as the control. (B) Immunohistochemical assessment of p-mTOR in the lung, intestine, and skeletal muscle of the OLD^{12M} and OLD^{RW} groups. Top, representative images; bottom, percentage of p-mTOR-positive cells and area. Scale bars: lung and skeletal muscle, 25 μm; intestine, 50 μm. (C) Immunofluorescence of p-S6 in the lung and small intestine in the OLD^{12M} and OLD^{RW} groups. Top, representative images; bottom, statistics. Scale bars: lung and small intestine, 25 μm. The data are presented as the means ± SEMs ($n = 3$ mice per group). ns, not significant; unpaired Student's *t* test. **FIGURE S4:** Effect of rapamycin withdrawal on stem cell number and proliferation in the mouse lung, skeletal muscle, and small intestine. (A-C) Representative immunostaining images of (A) $AT2^{pro\text{-}SPC}$ (red), (B) $MUSCs^{PAX7}$ (red), and (C) ISC^{LGR5} (green) in the lung, skeletal muscle, and small intestine of OLD^{12M} and OLD^{RW} mice. Five random alveolar areas, muscle fibers, or crypts were quantified. Scale bars, 25 μm. (D-E) Quantification of (D) $AT2^{pro\text{-}SPC}$-PCNA-positive and (E) Crypt-PCNA-positive cells, with representative images (left) and statistics (right). Scale bars for the lung and small intestine: 25 μm. The data are expressed as the means ± SEMs ($n = 3$ mice per group). ns, not significant; unpaired Student's *t* test. **FIGURE S5:** Effect of rapamycin withdrawal on stem cell differentiation in the mouse lung and small intestine. (A) Representative images of $AT2^{pro\text{-}SPC}$ (red) and $AT1^{HOPX}$ (green) immunostaining in the lungs of OLD^{12M} and OLD^{RW} mice and quantification of $AT1^{HOPX}$-positive cells. Scale bars, 25 μm. The white arrowheads indicate $AT1^{HOPX}$-positive cells. (B) Representative images of $Paneth^{LYZ}$ (red) immunostaining in the intestines of OLD^{12M} and OLD^{RW} and quantification of $Paneth^{LYZ}$-positive cells. Scale bars of $Paneth^{LYZ}$, 25 μm. The data are expressed as the means ± SEMs ($n = 3$ mice per group). $*p < 0.05$, $**p < 0.01$, $***p < 0.001$, ns, not significant; unpaired Student's *t* test. **Data S1:** Supplementary Tables.